Atmos. Chem. Phys. Discuss., 15, 15621–15654, 2015
www.atmos-chem-phys-discuss.net/15/15621/2015/
doi:10.5194/acpd-15-15621-2015

Atmospheric Chemistry and Physics Discussions

Black carbon concentrations and mixing state in the Finnish Arctic

T. Raatikainen, D. Brus, A.-P. Hyvärinen, J. Svensson, E. Asmi, and H. Lihavainen

Finnish Meteorological Institute, Helsinki, Finland

Received: 9 April 2015 – Accepted: 23 May 2015 – Published: 11 June 2015

Correspondence to: T. Raatikainen (tomi.raatikainen@fmi.fi)

Published by Copernicus Publications on behalf of the European Geosciences Union.

Abstract

Atmospheric aerosol composition was measured using a Single Particle Soot Photometer (SP2) in the Finnish Arctic during winter 2011–2012. The Sammaltunturi measurement site at the Pallas GAW (Global Atmosphere Watch) station receives air masses from different source regions including the Arctic Ocean and continental Europe. ~~SP2~~ is a unique instrument that can give detailed information about mass distributions and mixing state of refractory black carbon (rBC). As expected, the measurements showed widely varying rBC mass concentrations (0–120 ng m^{-3}), which were related to varying contributions of different source regions and aerosol removal processes. The log-normally distributed rBC core size was relatively constant with an average geometric mass mean diameter of 194 nm. On the average, the number fraction of particles containing rBC was 0.24 and the average rBC core size in these particles was half of the total size (coated to core diameter ratio was 2.0). These numbers mean that the core was larger and had a significantly thicker coating than in typical particles closer to their source regions. Comparison of the measured rBC mass concentration with that of the optically detected equivalent black carbon (eBC) showed a factor of five difference, which could not be fully explained without assuming that a part of the absorbing material is non-refractory. Finally, climate implications of five different rBC mixing state representations were quantified using the Mie approximation and simple direct radiative forcing efficiency calculations. These calculations showed that the observed mixing state (separate non-absorbing and coated rBC particles) means significantly lower warming effect or even a net cooling effect when compared with that of an homogenous aerosol containing the same amounts of rBC and non-absorbing material.

1 Introduction

Most atmospheric aerosols scatter incoming solar radiation and therefore have a cooling effect on climate, but especially black carbon aerosols absorb solar radiation, which means that they have a warming effect (IPCC, 2013; Bond et al., 2013). Absorbing aerosols have the largest warming effect over reflective surfaces such as clouds, snow and ice. In addition, deposition of absorbing aerosols on snow and ice decreases surface reflectivity which further enhances snow melt and decreases surface reflectivity (e.g., Hansen and Nazarenko, 2004; Flanner et al., 2007; Svensson et al., 2015). Most of the submicron aerosol absorption is caused by the broadly defined black carbon (BC), but there are also organic ~~compounds~~ that absorb especially at ultraviolet wavelengths (so-called brown carbon) and dust which is the main absorbing aerosol type for super micron particles (Bond et al., 2013). Atmospheric general circulation models are used to quantify climate effects of BC aerosols, but it is known that these models are not ~~always~~ accurate in simulating the complex aerosol lifecycles including formation, aging, transportation, cloud interactions, and removal processes (e.g., Kipling et al., 2013; Stohl et al., 2013; Genberg et al., 2013; Dutkiewicz et al., 2014; Wang et al., 2014a). This means that the model predicted aerosol concentrations and mixing state are not ~~always~~ in agreement with the observations. Detailed aerosol composition and mixing state measurements are therefore needed to assess model accuracies and to improve model ~~parameters~~ (Reddington et al., 2013; Schwarz et al., 2013; Samset et al., 2014; Wang et al., 2014b).

Aerosol interactions with radiation and water vapor depend on the mixing state of the absorbing material (e.g., Cappa et al., 2012). For example, it can be distributed so that a large fraction of particles contain small amounts of absorbing material or vice versa. By definition, an aerosol population is externally mixed when not all particles are absorbing and internally mixed when all particles are absorbing. Individual particles can also have different structures such as bare or coated black carbon particle or a homogenous mixture of black carbon and non-absorbing compounds. For the unit mass

of an absorbing material, internally mixed coated particles absorb more than externally mixed bare particles due to the increased effective cross sectional area (e.g., Schwarz et al., 2008b). In addition, aerosol interactions with water vapor, which are important for optical properties of droplets and clouds as well as for wet removal processes, depend on the mixing state (e.g., Zhang et al., 2008; Liu et al., 2013). For example, the capability of the initially hydrophobic black carbon particle to act as a cloud condensation nuclei (CCN) increases ~~with increasing coating thickness~~.

There are several instruments for measuring total black carbon concentrations, but few instruments are able to give any information about the mixing state. The Single Particle Soot Photometer or briefly SP2 (Stephens et al., 2003; Schwarz et al., 2006; Moteki et al., 2007) is probably the most versatile and widely used instrument for measuring mass distributions and mixing state of refractory black carbon (rBC). Refractory black carbon is the fraction of the absorbing carbonaceous material that has boiling point close to 4000 K and emits visible light when heated to that temperature (Petzold et al., 2013; Lack et al., 2014). This means that non-refractory absorbing material such as brown carbon cannot be detected by the SP2.

Long term ~~black carbon~~ measurements by thermal-optical methods show that concentrations have been decreasing in the Finnish Arctic during the last four decades (Dutkiewicz et al., 2014). On the annual scale, the highest ~~BC~~ concentrations are seen during winter and early spring (Hyvärinen et al., 2011; Dutkiewicz et al., 2014). ~~M~~Modelling study by Stohl et al. (2013) showed that the majority of the observed ~~black carbon~~ is from domestic combustion, but industrial sources and long-range transport have also a significant effect. Although there are a few previous airborne SP2 measurements covering the Arctic (e.g., Samset et al., 2014), they provide a snapshot of rBC mixing state at a specific altitude and location. Long term surface measurements are also needed as they provide boundary conditions for the vertical distributions and also show how concentrations vary as a function of time (diurnal and annual cycles, aerosol sources and removal processes).

The main purpose of this study is to provide new experimental information about the rBC mass distributions and mixing state ~~at~~ the Finnish Arctic. The SP2 measurements were conducted at Pallas GAW (Global Atmosphere Watch) station from December 2011 to February 2012. To our knowledge, these are the first published long-term surface SP2 results from the area and also from the Fennoscandian Arctic. In addition to the mixing state information, trajectory analysis is used to estimate the sources of rBC and the effects of different sources on rBC mixing state. We ~~will~~ also compare rBC concentrations with those from filter-based optical measurements to see if these are in agreement or depend on the physical properties (e.g. volatility) of black carbon. Finally, climate implications of different black carbon mixing state representations are assessed based on a Mie approximation and a simple direct radiative forcing efficiency model.

2 Experimental

2.1 Pallas measurement station

Figure 1 shows the location of the Pallas Global Atmosphere Watch (GAW) station at the northern edge of continental Europe. Measurements were conducted on a top of a fell called Sammaltunturi (67°58.400′ N 24°6.939′ E, 565 m a.m.s.l.) about 250 m above surrounding sparsely populated hilly terrain covered by mixed pine, spruce and birch forests (Hatakka et al., 2003). In the absence of significant local aerosol sources, most observed particles are long-range transported from the Kola Peninsula and from more densely populated and industrialized areas from the south. Therefore, Pallas is a site where relatively aged air masses can be observed on their way to the north. On the other hand, the site also receives clean air masses from the north.

2.2 Instrumentation

The station has ~~stationary~~ instruments for measuring meteorological parameters, trace gases and aerosol size distributions and optical properties. During the Pallas winter campaign, a Single Particle Soot Photometer (SP2; Revision C* with 8 channels) manufactured by Droplet Measurement Technologies (Boulder, CO, USA) was used to measure size distributions and mixing state of refractory black carbon (rBC). Brief description of the instrument, data processing and calculated parameters are given in Sect. "Single Particle Soot Photometer (SP2)".

The measurement station has three sample lines: one is without nominal cut-off diameter (the total line) and the other lines have about 5 µm (the gas line) and 10 µm (PM_{10} line) cut-off sizes. The SP2 was connected to the PM_{10} sample line, which means that some ice nuclei (IN) and cloud condensation nuclei (CCN) are not detectable when the station is covered by clouds. These in cloud time periods are found by comparing particle number size distributions from two Differential Mobility Particle Sizers (DMPS). One DMPS was connected to the total line (all particles) and the other was connected to the gas line (IN and CCN removed at the inlet). The difference between the total and gas sample line size distribution gives the size distribution of IN and CCN, which are typically larger than 100 nm in dry diameter. In our analysis, the relative difference (i.e. activated fraction) for 260–465 nm dry size range which is larger than 0.8 is considered as an in cloud case and a value smaller than 0.2 indicates clear conditions; the remaining points indicate missing DMPS data or unclear or variable cloud conditions.

Multiangle Absorption Photometer (MAAP) and seven-wavelength Aethalometer collect aerosols to a filter and measure the change in light attenuation. This is then converted to equivalent black carbon (eBC) mass concentration by using instrument specific parameters. MAAP data was used as is, but Weingartner correction (Weingartner et al., 2003) was applied to the Aethalometer data. The MAAP was connected to the same PM_{10} sample line as the SP2, which means that their reported eBC and rBC

concentrations are always comparable, but both can be biased during the in cloud conditions. The Aethalometer was connected to the total sample line.

Concentrations of carbon monoxide and dioxide (CO and CO_2), nitrogen dioxide (NO_2), sulfur dioxide (SO_2) and ozone (O_3) were measured using instruments described by Hatakka et al. (2003), except that CO and CO_2 are more recently measured by a Picarro CRDS (Cavity Ring-Down Spectroscopy) analyzer. Since some of these gases are co-emitted with the aerosol black carbon, comparison of rBC and gas concentrations can give an indication of rBC sources and the age of the air masses.

Single Particle Soot Photometer (SP2)

Detailed description of the instrument operation principles is given elsewhere (e.g., Stephens et al., 2003; Schwarz et al., 2006; Moteki et al., 2007). Briefly, sample aerosol particles travel through a powerful laser beam, where non-absorbing and absorbing particles are identified based on the scattered laser light and emissions of visible light (laser-induced incandescence), respectively. The maximum incandescence signal is proportional to the refractory black carbon (rBC) mass and this dependency is parameterized using size-selected Aquadag® (Acheson Inc., USA) particles, ~~which~~ masses are calculated using the density parameterization from Gysel et al. (2011). This calibration gives ambient rBC particle mass (0.4–260 fg) as a function of measured incandescence signal amplitude; rBC core volume equivalent diameter (75–655 nm sizing range) is then calculated from the mass by assuming 1800 kg m^{-3} particle density. Non-absorbing particles scatter laser light so that the maximum scattering signal is proportional to the scattering cross section of the particle, which is calculated using the Mie approximation (e.g., Bohren and Huffman, 1983). Again, calibration experiments are used to relate calculated scattering cross sections of size-selected ammonium sulfate particles to the observed scattering signal amplitudes. This calibration gives scattering cross sections for ambient particles, so their exact sizes depend on particle shape, structure and refractive index. In practice, we have assumed that ambient particles are

spherical and optically similar to ammonium sulfate even when they contain rBC. This means that the scattering particle sizing range is 190–535 nm.

Additional analysis is required to calculate sizes of coated rBC particles. The scattering signal is first Gaussian following the Gaussian laser beam profile, but reduces from that when the coating starts to evaporate. The unperturbed scattering signal amplitude can be reconstructed using so-called Leading Edge Only (LEO) method (Gao et al., 2007; Metcalf et al., 2012). In practice, a Gaussian scattering signal profile with known peak position and width is fitted to the Gaussian section of the observed scattering signal (the leading edge) by adjusting peak height. Peak positions and widths are obtained from those of purely scattering particles: the width is simply the width of the observed scattering signal and peak position is based on the observed lag time from a Two-Element Avalanche Photodiode (TEAPD) detector signal to the scattering peak position. In the current calculations, the widths and the lag times are calculated as a standard deviation weighted running mean using values from 100 previous purely scattering particles. The leading edge fit includes points where the Gaussian signal is between 1/1500 and 1/30 of the maximum value. LEO fits can be made when the leading edge scattering signal exceeds noise and the TEAPD signal is valid; for the current SP2 this means that coated particle size must be at least 300 nm.

Hourly average mass and number size distributions (40 logarithmic size bins) and mixing state parameters (number fraction of particles containing rBC and coated to core diameter ratios for those particles) are calculated from the single particle data. Concentrations are calculated using recorded sample flow rates at instrument temperature and pressure. The number fraction of rBC containing particles (N_{rBC}/N_{total}) is calculated from the rBC and non-absorbing particle number size distributions measured by the SP2. The number concentration of rBC containing particles (N_{rBC}) is calculated by integrating the rBC number size distribution over 350–450 nm LEO (or coated particle) size range. Similarly, the number concentration of non-absorbing particles (the total is the sum of rBC containing and non-absorbing particles) is calculated from the non-absorbing particle number size distribution using the same LEO size range (LEO

size used for consistency). The 350–450 nm integration LEO size range is selected considering LEO sizing limits and counting statistics. The lowest particle size (350 nm) is large enough so that reliable LEO fits can be made and the size range from 350 to 450 nm contains enough particles for reasonable counting statistics. In practice, this size range is representative of the typical coated accumulation mode rBC particles. The first results showed that practically all rBC particles are coated by a non-refractory material (core-shell structure assumed). Because absolute coating thickness depends on particle size so that larger particles have typically thicker coatings, a relative parameter is better for averaging. Here relative coating thickness is defined as coated (from LEO method) to core diameter ratio, D_p/D_{rBC}, and it is calculated as an average of those of individual rBC containing particles which rBC core diameter (D_{rBC}) is 150–200 nm. This 150–200 nm rBC core size range has enough particles for good counting statistics and it is in the range where typical coating thicknesses are accounted for.

The initial SP2 data analysis showed that some results were dependent on the SP2 chamber temperature, which ranged from 23 to 33 °C during the campaign. By comparing measured rBC concentration with the equivalent BC (eBC) measured by MAAP, it was concluded that the SP2 ~~undercounted~~ rBC when SP2 temperature decreased below 25 °C, so this SP2 data was ignored. Careful inspection of the SP2 data showed that laser power was most likely decreased below the minimum required for heating rBC particles to their boiling point. Namely, decreasing temperature and laser power meant that particles reached their boiling points closer to the center of the laser beam. This means that particles that miss the center of the laser beam (particle beam width is about 25 % of the laser beam width; Laborde et al., 2012b) do not always reach their incandescence temperature and therefore are not detected as rBC. When laser power is high enough, incandescence signal is practically independent of the laser power, but scattering signal is always proportional to the laser power. However, comparison of scattering particle size distributions and particle size distributions from DMPS showed that the instrument temperature could have caused about 10 % bias to the scattering size, which is smaller than the typical sizing uncertainty of the instrument. The weak

temperature dependency is partly explained by the fact that the scattering detector gain is also temperature dependent, but so that the gain (signal) increases when laser power decreases (SP2 workshop communications, Boulder, CO, USA, 2014). In addition, scattering size is proportional to the logarithm of the signal, so even a 50 % change in laser power would have a minor effect on scattering size.

2.3 Trajectories

Five days ~~long~~ backward trajectories were calculated using the HYSPLIT model (Draxler and Hess, 1997, 1998; Draxler, 1999). Trajectory end point altitude was set to 500 m a.g.l. Trajectory calculations were initiated every three hours and coordinate points were saved hourly (120 coordinate points in addition to the end point). Each trajectory is represented by two parameters: average distance and direction. These are the magnitude and direction of a vector calculated as an average of vectors pointing from Pallas to each of the hourly trajectory coordinate points. The vectors from Pallas to the trajectory coordinate points were initially converted from spherical (latitude and longitude degrees) to Cartesian coordinates (kilometers). Average distance and direction indicate the distance and direction of the source area from the Pallas measurement station, respectively. Trajectories originating from Central Europe and southern Finland have similar average directions, but these can be distinguished based on the average distance.

3 Results

3.1 Meteorology

Ambient temperature was initially about −2 °C, but decreased throughout the campaign reaching −24 °C at the end. Snowfall was observed occasionally, but these and visibility observations were missing from most days (32 % data coverage). ~~C~~campaign average

wind speed was 9 m s^{-1} and the hourly averages were between 1 and 17 m s^{-1}. The S–SW was the most frequent wind direction sector and the second was NE–E. Trajectory analysis gave slightly different view of the origin of the air masses with dominating sector centered at SE (Eastern Europe) and a minor sector at E (Kola Peninsula). The campaign started 17 December 2011 during the polar night, which lasts about 3.5 weeks at that location, but at the end of the campaign (2 February 2012) the daily maximum solar radiation reached 30 W m^{-2}.

3.2 rBC properties

Figure 2 shows campaign averages of rBC mass and number size distributions. The number size distribution extends well below 75 nm detection limit, which means that distribution parameters (total number, mode and width) cannot be calculated or determined from a fit to the data. On the other hand, the observed rBC mass seem to be centered within the sizing range (75–655 nm). For example, using the log-normal fit to extrapolate rBC mass concentration would give 27 ng m^{-3} when the integrated rBC mass is 26 ng m^{-3}. Therefore, calculated log-normal mass distribution parameters (total mass concentration, geometric mass mean diameter and geometric standard deviation) will be used to describe rBC mass distribution. Because geometric standard deviation is fairly constant, we will focus on the total mass concentration and geometric mass mean diameter.

Figure 3 shows the time series of the main rBC properties including the total mass concentration (c_{rBC}), geometric mass mean diameter (GMD_{rBC}), number fraction of particles containing rBC (N_{rBC}/N_{total}), and ~~coated~~ to core diameter ratio (D_p/D_{rBC}). Background color indicates when the station is in cloud (blue) and when not (red), and when the presence of clouds is unclear or the DMPS data is missing (white). As explained in Sect. 2.2, SP2 measurements can be biased during the in cloud time periods, because some ice and cloud condensation nuclei become too large to be detected. There are some cases where the changes in the observed aerosol parameters

can be related to the appearance or disappearance of clouds, but most of the observed variability is caused by other factors such as air mass history. Statistical analysis (not shown) was also performed to confirm that the average aerosol properties were similar during no cloud and in cloud time periods. Therefore, we will use the full data set in the following calculations.

Average rBC mass concentration is 26 ng m^{-3}, but the values range from about zero to 120 ng m^{-3} (Fig. 3). Average geometric mass mean diameter is 194 nm and 90 % of the values are between 161 and 231 nm. The average number fraction of particles containing rBC is 0.24 and again 90 % of the values are between 0.14 and 0.35. Finally, the average ~~coated~~ to core diameter ratio is 2.0 and the 90 % limits are from 1.8 to 2.1. Although ~~especially~~ mass concentration varies significantly, rBC number fraction and ~~coated~~ to core diameter ratio have relatively constant values.

3.2.1 Comparison with other SP2 studies

One complication in comparing SP2 results is that different calibration materials are being used (e.g. Aquadag® or fullerene soot; Moteki and Kondo, 2010; Laborde et al., 2012a; Baumgardner et al., 2012) and different optical and physical properties (e.g. refractive index, particle structure and density) are assumed for the ambient rBC and scattering material. There are also different ways to calculate mixing state parameters (e.g. size range). To our knowledge, this is the first published SP2 study where long-term surface measurements have been conducted at high latitudes during Arctic winter, so direct comparison with other studies is not possible. Nevertheless, published studies can give an idea of how Pallas rBC properties are related to those from different environments.

In general, rBC observed at Pallas is long-range transported and aged. As a result, rBC mass concentrations are lower and particles are larger than in air masses observed closer to their source regions (e.g., Huang et al., 2012; Reddington et al., 2013; McMeeking et al., 2010). Although rBC mass concentrations and mean diameters are commonly reported, there is less information about the rBC mixing state (rBC

coating thickness and number fraction of rBC containing particles). Previous airborne measurements have shown that the relative coating thickness (D_p/D_{rBC}) is typically close to 1.5 in long-range transported urban and biomass burning plumes (e.g., Kondo et al., 2011; Schwarz et al., 2008a; Sahu et al., 2012; Metcalf et al., 2012), which is significantly smaller than the 2.0 observed at Pallas. There is very little published information about the number fraction of particles containing rBC especially at the aged air masses. The closest match with our study is the study of Reddington et al. (2013) who used rBC measurements and model information to estimate that 14 % of particles larger than 260 nm contain rBC in the European lower troposphere (altitude less than 2.5 km above ground level). This fraction is again significantly smaller than the 24 % observed at Pallas. One possible explanation is that cloud processing increases rBC coating thickness (condensation of semi-volatile species and coagulation) and removes more hygroscopic particles (wet deposition) during the transport from source areas to Pallas.

In addition to the basic mixing state parameters, careful examination of the scattering and incandescence signals can show if the rBC particles are coated or not and if the particles have core-shell structure. For example, Huang et al. (2012) summarizes number fractions of coated (called internally mixed in their paper) rBC from several studies (environments) and shows that the number fraction varies between 3 and 80 %. Although different calculation methods can lead to lower values (thin coatings cannot be detected from small rBC particles), these numbers are much smaller than that observed at Pallas where practically 100 % of rBC particles are coated (bare rBC was not observed). There are also studies where rBC containing particles have disintegrated in the laser beam, which has been interpreted either as a result of very thick coatings (Dahlkötter et al., 2014) or that the rBC is attached to the surface or is close to the surface of a non-absorbing particle (Sedlacek et al., 2012; Moteki et al., 2014), but such behavior was not observed at Pallas.

3.2.2 Diurnal variations

Due to the high variability of the rBC parameters, statistically significant diurnal cycles were not observed (not shown). This is not surprising as diurnal variations of solar radiation and temperature are minimal during the Arctic winter. However, when diurnal cycles are calculated separately for the polar night and the following early spring, weak diurnal cycles can be observed in rBC mass concentration, but not in the other aerosol parameters. During the polar night, rBC mass concentration peaks during midnight, which could refer to regional emissions. After the polar night, rBC concentration has the maximum during local midday followed by an afternoon decrease, which can be explained by dilution when mixing layer height increases. In general, other factors such as source region and removal processes during the transport time are more important for the variability of both rBC mass and mixing state parameters especially during winter.

3.3 Correlation with other observations

Most of the rBC parameters have rapid variations (see Fig. 3) compared with the time scales of variations of the observed trace gas concentrations (CO, CO_2, NO_2, SO_2 and O_3), meteorological parameters (temperature, pressure, and wind direction and speed) and computed backward trajectories. However, at least rBC mass concentration trends can be correlated with certain trace gases and trajectory or wind directions. The other parameters such as rBC geometric mass mean diameter, number fraction and coating thickness seemed to be less dependent on the weather and trajectory parameters and concentrations of the trace gases.

From the trace gases, the best correlations are seen between rBC mass and CO, NO_2 and CO_2 concentrations as these are co-emitted during different combustion processes. Carbon monoxide (CO) is the most commonly used tracer, so we will focus on that. Pearson's correlation coefficient for a linear fit between rBC and CO is 0.74, slope $\Delta rBC/\Delta CO$ is 0.742 $ng\,m^{-3}\,ppb^{-1}$ ($ppb = nmol\,mol^{-1}$) and the background CO concen-

tration (CO concentration where rBC concentration is zero) is 126 ppb. ΔrBC/ΔCO values depend on the aerosol source and the age of the air mass (e.g., McMeeking et al., 2012). Current ΔrBC/ΔCO value is lower than that from most other SP2 studies focusing on fresh biomass burning, industrial and urban plumes (e.g., McMeeking et al., 2010; Kondo et al., 2011; Baumgardner et al., 2007; McMeeking et al., 2012; Sahu et al., 2012). Instead of having different rBC and CO sources, the low ΔrBC/ΔCO value observed at Pallas is more likely the result of aging of the air masses during the transport from source regions to Pallas. The ratio decreases during the transport due to the extended CO lifetime (low levels of solar radiation) and efficient removal of the relatively hydrophilic thickly coated rBC during the rainy and cloudy winter months. Similar and even lower ΔrBC/ΔCO values have been observed in free troposphere background air and in air masses that have been experiencing heavy precipitation (Liu et al., 2010; Matsui et al., 2011).

It is assumed that the calculated average trajectory directions describe the origin of air masses better than the measured local wind directions. Therefore, Fig. 4 shows rBC mass concentration (here 3 h averages) as a function of average trajectory direction. The trajectory directions can be divided into three source regions: Arctic Ocean, Continental Europe and North Atlantic. Each data point is also colored based on the average trajectory distance from the measurement location. In good agreement with the expectations, the figure shows that rBC concentrations are low when air masses are originating from North Atlantic or Arctic Ocean, and the highest concentrations are observed when trajectories are originating from the southern sector and especially from Eastern Europe (average distance more than 1000 km). The lowest concentrations in this polluted sector are observed when air masses are originating mainly from Southern Finland and the Baltic Countries (average distance less than 1000 km). Again, rBC number fractions and coating thicknesses seemed to be independent of air mass origin. Especially coating thickness could have been dependent on rBC source region (age), which was not observed, but it is possible that this data set is too short for finding such dependencies.

3.4 Refractory and equivalent black carbon

MAAP and Aethalometer use optical methods to measure aerosol absorption coefficients which are converted to equivalent BC (eBC) mass concentrations. Figure 5 shows correlations between these two and rBC concentration measured by the SP2. The Aethalometer and MAAP eBC concentrations are in good agreement when the Pallas measurement site is not in cloud (circled data points). During the in cloud conditions, the PM_{10} (humid size) eBC measured by MAAP is 30–100 % of the total eBC measured by the Aethalometer. PM_{10} and total eBC concentrations can be similar during the in cloud conditions if ice particle and cloud droplet sizes are smaller than 10 µm or other than eBC containing particles have been activating.

The rBC is about 20 % of the eBC measured by MAAP (both PM_{10}), but the fraction is practically constant. The factor of five difference between eBC and rBC is unexpected, but smaller differences are possible. For example, our unpublished laboratory experiments with this same SP2 have shown a factor of two difference for Aquadag® aerosol. There are several potential reasons for the observed difference. First of all, rBC is a fraction of eBC, which can contain non-refractory light absorbing organics such as brown carbon. Secondly, MAAP detects practically all absorbing particles, but SP2 sizing is limited to 75–655 nm rBC core diameter range. Although larger particles, which saturate the incandescence detectors, were rarely observed, rBC particles smaller than 75 nm can also have a non-negligible mass. Third, thick non-refractory coatings can increase absorption and MAAP eBC mass due to the lensing effect, but SP2 results are independent of the coatings (Slowik et al., 2007). Fourth, these instruments have composition dependent parameters (mass absorption coefficient (MAC) for MAAP and incandescence efficiencies of the calibration and ambient rBC for SP2), which optimal values might differ from the used default values. Default MAC (6.6 $m^2 g^{-1}$) was used in Pallas MAAP data analysis, but larger values up to factor of two have been reported (e.g., Liu et al., 2010; Lack et al., 2014). Current SP2 was calibrated using Aquadag®, but using a specific batch of fullerene soot which represents ambient aerosol in Tokyo

(Moteki and Kondo, 2010) would have given about 33 % larger rBC mass for the same measured incandescence signal (Laborde et al., 2012b, a). Although these instrument parameters can explain a large fraction of the factor of five differences between eBC and rBC, it is likely that some fraction of the total absorbing aerosol mass in Pallas is non-refractory material such as brown carbon.

3.5 Climate implications

In this section we will quantify the effect of black carbon mixing state on aerosol radiative properties when the total aerosol composition is known (from our measurements described in the previous sections). From the various mixing state representations (see e.g., Lang-Yona et al., 2010), we have selected the one that matches with the current observations and four other that are in common use. The five mixing state representations include two internally mixed (only one particle type containing both absorbing and non-absorbing material) and three externally mixed (separate absorbing and non-absorbing particle types) aerosol populations. The internally mixed particles can be homogenous (INT-HOM) or absorbing cores with a non-absorbing coating (INT-COAT). The externally mixed particles have always one non-absorbing and one absorbing size distribution. The absorbing particles can be bare absorbing material (EXT-BARE), coated absorbing cores (EXT-COAT) or a homogenous mixture of the absorbing and non-absorbing components (EXT-HOM). The EXT-COAT case is the one based on our observations.

All model calculations are based on the same total particle size distribution and chemical composition (campaign averages), but the absorbing and non-absorbing species are distributed differently according to the mixing state representation. Based on our measurements, the average total rBC mass concentration is 26 ng m^{-3}, the number fraction of particles containing rBC is 0.24 and coated to (refractory) core diameter ratio is 2.0. This means that the total rBC volume fraction is ($0.24/2.0^3$ =) 0.03 and the rest is non-refractory material. Also, the total volume of all particles must be 460×10^{-9} cm^3 m^{-3} based on the observed rBC mass concentration (density is

1800 kg m^{-3}) and volume fraction (0.03). Because SP2 does not detect scattering particles smaller than 190 nm, particle size distribution parameters are obtained from the gas line DMPS measurements: geometric volume mean diameter and standard deviation are 323 nm and 1.54, respectively. Volume distribution is used here, because particles larger than 100 nm have the dominant effect on light absorption and scattering. As described in Sect. 3.4, significant fraction of the absorbing material is likely to be non-refractory. Therefore, the absorbing component of the non-refractory material is here considered as light absorbing carbon (LAC) and it's volume fraction is calculated from that of the eBC (eBC = rBC + LAC) measured by the MAAP. Based on the average rBC to eBC ratio of 0.21, eBC volume fraction is 0.15, which means that LAC volume fraction is 0.12. The rest of the total volume is assumed to be ammonium sulfate. Optical constants of the different particle types are calculated as a volume fraction weighted average of those of the pure compounds. The complex refractive indices of ammonium sulfate, LAC and rBC are $1.51 + 0i$, $1.95 + 0.79i$ Baumgardner et al. (2007) and $2.26 + 1.26i$ (Moteki et al., 2010), respectively. For example, in the EXT-COAT case, 24 % of the particles contain absorbing material and the rest are pure ammonium sulfate. The absorbing particles contain a core, which is composed of a mixture of rBC ($1/2.0^3$ of the particle volume) and LAC ($0.12/0.03 \cdot 1/2.0^3$ of the particle volume), and the coating is ammonium sulfate.

Numerical calculations using the Bohren and Huffman (1983) BHMIE and BHCOAT codes give extinction (b_{ext}) and absorption coefficients (b_{abs}) and backscatter fraction (b) for the particle populations at 550 nm wavelength. These are the main parameters in an equation for global mean top of atmosphere radiative forcing efficiency (RFE) per unit optical depth (Haywood and Shine, 1995; Anderson et al., 1999):

$$\mathrm{RFE} = SD(1 - A_{\mathrm{c}})T_{\mathrm{a}}^2(1 - R_{\mathrm{s}})^2 \left(\frac{2R_{\mathrm{s}}(1 - \omega)}{(1 - R_{\mathrm{s}})^2} - \beta\omega \right) \quad (1)$$

The parameters are solar constant (S = 1370 W m^{-2}), annual average daylight fraction (D = 0.5), fractional cloud coverage (A_{c} = 0.6), atmospheric transmissivity (T_{a} = 0.87),

surface albedo (R_s=0.2), single scattering albedo ($\omega = 1 - b_{abs}/b_{ext}$), and average upscatter fraction (β). The upscatter fraction is parameterized as a function of backscatter fraction b: $\beta = 0.082 + 1.85b - 2.97b^2$ (Anderson et al., 1999).

The results of the calculations, which include extinction and absorption coefficients and backscatter fraction used in Eq. (1), are given in Table 1. Because the absorbing material is distributed over all internally mixed aerosol particles, which means larger effective absorption cross section, this aerosol is more absorbing and less scattering than the externally mixed aerosol (e.g., Cappa et al., 2012). Compared with the overall difference between the internally and externally mixed aerosol, the difference between core-shell and homogenous particle types is small. Mainly due to the differences in single scattering albedo, RFE values are positive (warming effect) for the internally mixed aerosol and negative (cooling effect) for the externally mixed aerosol. As the current and most other experimental results show that at least the aged rBC is externally mixed, assuming an internal mixture would lead to overestimated climate warming effect.

4 Conclusions

We have measured refractory black carbon (rBC) mass distributions and mixing state by using a Single Particle Soot Photometer (SP2) at an Arctic measurement site in Northern Finland. To our knowledge, these are the first published surface SP2 measurements made in the Fennoscandian Arctic. The results show that rBC mass concentrations are relatively low (average mass concentration 26 ng m^{-3}) and most of the rBC is long-range transported from south. Observed particles are larger (geometric mass mean diameter 194 nm) than those observed close to the source regions. On the average, 24 % of the accumulation mode particles contain an observable (diameter at least 75 nm) rBC core. These particles are thickly coated with the average coated to core diameter ratio 2.0; bare rBC particles or other than core-shell structures were not observed.

From the rBC mass distributions and mixing state parameters only the mass concentration was clearly correlated with co-emitted trace gases including carbon monoxide (CO), carbon dioxide (CO_2) and nitrogen dioxide (NO_2). The correlation of rBC with CO showed shallow slope, which was interpreted as a result of relatively aged air masses where rBC has been removed mainly by wet deposition. Similarly, rBC mass concentration was also the only parameter that correlated with air mass history described by the average directions and lengths of backward trajectories. The largest concentrations were observed when the trajectories were originating from Eastern Europe and the lowest concentrations were from North Atlantic and Arctic Ocean.

SP2 measurements provided detailed information about the rBC mixing state, but different mixing states have been used in various aerosol models. The effect of rBC mixing state on aerosol radiative properties were estimated by using a Mie approximation and a simple direct radiative forcing efficiency calculations. The difference between core-shell and homogenous particle structures is small compared with that between internally (all particles have an absorbing component) and externally (a fraction of particles have an absorbing component) mixed aerosol populations. The internally mixed aerosol is more absorbing due to the higher effective absorbing cross sectional area, which means that these aerosols are more likely to have a warming effect. However, the same aerosol can have a cooling effect when assuming externally mixed absorbing and non-absorbing particles. Our current and most other observations show that especially the aged absorbing aerosol is externally mixed (a fraction of particles are absorbing), which means that assuming an internally mixed homogenous aerosol means overestimated aerosol warming effect.

Current radiative forcing calculations are highly simplified, so more detailed model calculations should be done to obtain a more realistic radiative forcing estimate. Before that can be done, accurate measurements are needed to develop a global picture of the mixing state of the absorbing aerosol. Long term measurements are also needed to observe the diurnal and annual cycles. SP2 is probably the best instrument for that

purpose, but this requires consistent use of data analysis methods and reference materials.

Acknowledgements. This work was supported by the EU LIFE+ project MACEB (project no. LIFE09 ENV/FI/000572), the Academy of Finland project Greenhouse gas, aerosol and albedo variations in the changing Arctic (project number 269095), the Academy of Finland through the FCoE in Physics, Chemistry, Biology and Meteorology of Atmospheric Composition and Climate Change (program numbers 1118615 and 272041), black and brown carbon influence on climate and climate change in India – from local to regional scale (project no. 264242), Arctic Absorbing Aerosols and Albedo of Snow (project no. 3162), the Nordic research and innovation initiative CRAICC, and KONE foundation. We would also like to thank J. Hatakka and T. Laurila for providing the gas data.

References

Anderson, T. L., Covert, D. S., Wheeler, J. D., Harris, J. M., Perry, K. D., Trost, B. E., Jaffe, D. J., and Ogren, J. A.: Aerosol backscatter fraction and single scattering albedo: Measured values and uncertainties at a coastal station in the Pacific Northwest, J. Geophys. Res., 104, 26793–26807, 1999. 15638, 15639

Baumgardner, D., Kok, G. L., and Raga, G. B.: On the diurnal variability of particle properties related to light absorbing carbon in Mexico City, Atmos. Chem. Phys., 7, 2517–2526, doi:10.5194/acp-7-2517-2007, 2007. 15635, 15638

Baumgardner, D., Popovicheva, O., Allan, J., Bernardoni, V., Cao, J., Cavalli, F., Cozic, J., Diapouli, E., Eleftheriadis, K., Genberg, P. J., Gonzalez, C., Gysel, M., John, A., Kirchstetter, T. W., Kuhlbusch, T. A. J., Laborde, M., Lack, D., Müller, T., Niessner, R., Petzold, A., Piazzalunga, A., Putaud, J. P., Schwarz, J., Sheridan, P., Subramanian, R., Swietlicki, E., Valli, G., Vecchi, R., and Viana, M.: Soot reference materials for instrument calibration and intercomparisons: a workshop summary with recommendations, Atmos. Meas. Tech., 5, 1869–1887, doi:10.5194/amt-5-1869-2012, 2012. 15632

Bohren, C. and Huffman, D. R.: Absorption and scattering of light by small particles, Wiley, New York, 1983. 15627, 15638

Bond, T. C., Doherty, S. J., Fahey, D. W., Forster, P. M., Berntsen, T., DeAngelo, B. J., Flanner, M. G., Ghan, S., Kärcher, B., Koch, D., Kinne, S., Kondo, Y., Quinn, P. K., Sarofim, M. C.,

Schultz, M. G., Schulz, M., Venkataraman, C., Zhang, H., Zhang, S., Bellouin, N., Guttikunda, S. K., Hopke, P. K., Jacobson, M. Z., Kaiser, J. W., Klimont, Z., Lohmann, U., Schwarz, J. P., Shindell, D., Storelvmo, T., Warren, S. G., and Zender, C. S.: Bounding the role of black carbon in the climate system: A scientific assessment, J. Geophys. Res., 118, 5380–5552, doi:10.1002/jgrd.50171, 2013. 15623

Cappa, C. D., Onasch, T. B., Massoli, P., Worsnop, D. R., Bates, T. S., Cross, E. S., Davidovits, P., Hakala, J., Hayden, K. L., Jobson, B. T., Kolesar, K. R., Lack, D. A., Lerner, B. M., Li, S.-M., Mellon, D., Nuaaman, I., Olfert, J. S., Petäjä, T., Quinn, P. K., Song, C., Subramanian, R., Williams, E. J., and Zaveri, R. A.: Radiative Absorption Enhancements Due to the Mixing State of Atmospheric Black Carbon, Science, 337, 1078–1081, doi:10.1126/science.1223447, 2012. 15623, 15639

Dahlkötter, F., Gysel, M., Sauer, D., Minikin, A., Baumann, R., Seifert, P., Ansmann, A., Fromm, M., Voigt, C., and Weinzierl, B.: The Pagami Creek smoke plume after long-range transport to the upper troposphere over Europe – aerosol properties and black carbon mixing state, Atmos. Chem. Phys., 14, 6111-6137, doi:10.5194/acp-14-6111-2014, 2014. 15633

Draxler, R.: HYSPLIT4 user's guide, NOAA Tech. Memo. ERL ARL-230, NOAA Air Resources Laboratory, Silver Spring, MD, 1999. 15630

Draxler, R. and Hess, G.: Description of the HYSPLIT_4 modeling system., NOAA Tech. Memo. ERL ARL-224, NOAA Air Resources Laboratory, Silver Spring, MD, 24 pp., 1997. 15630

Draxler, R. and Hess, G.: An overview of the HYSPLIT_4 modeling system of trajectories, dispersion, and deposition, Aust. Meteorol. Mag., 47, 295–308, 1998. 15630

Dutkiewicz, V. A., DeJulio, A. M., Ahmed, T., Laing, J., Hopke, P. K., Skeie, R. B., Viisanen, Y., Paatero, J., and Husain, L.: Forty-seven years of weekly atmospheric black carbon measurements in the Finnish Arctic: Decrease in black carbon with declining emissions, J. Geophys. Res., 119, 7667–7683, doi:10.1002/2014JD021790, 2014. 15623, 15624

Flanner, M. G., Zender, C. S., Randerson, J. T., and Rasch, P. J.: Present-day climate forcing and response from black carbon in snow, J. Geophys. Res., 112, D11202, doi:10.1029/2006JD008003, 2007. 15623

Gao, R. S., Schwarz, J. P., Kelly, K. K., Fahey, D. W., Watts, L. A., Thompson, T. L., Spackman, J. R., Slowik, J. G., Cross, E. S., Han, J.-H., Davidovits, P., Onasch, T. B., and Worsnop, D. R.: A Novel Method for Estimating Light-Scattering Properties of Soot Aerosols Using a Modified Single-Particle Soot Photometer, Aerosol Sci. Tech., 41, 125–135, doi:10.1080/02786820601118398, 2007. 15628

Genberg, J., Denier van der Gon, H. A. C., Simpson, D., Swietlicki, E., Areskoug, H., Beddows, D., Ceburnis, D., Fiebig, M., Hansson, H. C., Harrison, R. M., Jennings, S. G., Saarikoski, S., Spindler, G., Visschedijk, A. J. H., Wiedensohler, A., Yttri, K. E., and Bergström, R.: Light-absorbing carbon in Europe – measurement and modelling, with a focus on residential wood combustion emissions, Atmos. Chem. Phys., 13, 8719–8738, doi:10.5194/acp-13-8719-2013, 2013. 15623

Gysel, M., Laborde, M., Olfert, J. S., Subramanian, R., and Gröhn, A. J.: Effective density of Aquadag and fullerene soot black carbon reference materials used for SP2 calibration, Atmos. Meas. Tech., 4, 2851–2858, doi:10.5194/amt-4-2851-2011, 2011. 15627

Hansen, J. and Nazarenko, L.: Soot climate forcing via snow and ice albedos, P. Natl. Acad. Sci. USA, 101, 423–428, doi:10.1073/pnas.2237157100, 2004. 15623

Hatakka, J., Aalto, T., Aaltonen, V., Aurela, M., Hakola, H., Komppula, M., Laurila, T., Lihavainen, H., Paatero, J., Salminen, K., and Viisanen, Y.: Overview of the atmospheric research activities and results at Pallas GAW station, Boreal Environ. Res., 8, 365–383, 2003. 15625, 15627

Haywood, J. M. and Shine, K. P.: The effect of anthropogenic sulfate and soot aerosol on the clear sky planetary radiation budget, Geophys. Res. Lett., 22, 603–606, doi:10.1029/95GL00075, 1995. 15638

Huang, X.-F., Sun, T.-L., Zeng, L.-W., Yu, G.-H., and Luan, S.-J.: Black carbon aerosol characterization in a coastal city in South China using a single particle soot photometer, Atmos. Environ., 51, 21–28, 2012. 15632, 15633

Hyvärinen, A.-P., Kolmonen, P., Kerminen, V.-M., Virkkula, A., Leskinen, A., Komppula, M., Hatakka, J., Burkhart, J., Stohl, A., Aalto, P., Kulmala, M., Lehtinen, K., Viisanen, Y., and Lihavainen, H.: Aerosol black carbon at five background measurement sites over Finland, a gateway to the Arctic, Atmos. Environ., 45, 4042–4050, 2011. 15624

Kipling, Z., Stier, P., Schwarz, J. P., Perring, A. E., Spackman, J. R., Mann, G. W., Johnson, C. E., and Telford, P. J.: Constraints on aerosol processes in climate models from vertically-resolved aircraft observations of black carbon, Atmos. Chem. Phys., 13, 5969–5986, doi:10.5194/acp-13-5969-2013, 2013. 15623

Kondo, Y., Matsui, H., Moteki, N., Sahu, L., Takegawa, N., Kajino, M., Zhao, Y., Cubison, M. J., Jimenez, J. L., Vay, S., Diskin, G. S., Anderson, B., Wisthaler, A., Mikoviny, T., Fuelberg, H. E., Blake, D. R., Huey, G., Weinheimer, A. J., Knapp, D. J., and Brune, W. H.: Emissions of black carbon, organic, and inorganic aerosols from biomass burning in North America and

Asia in 2008, J. Geophys. Res., 116, D08204, doi:10.1029/2010JD015152, 2011. 15633, 15635

Laborde, M., Mertes, P., Zieger, P., Dommen, J., Baltensperger, U., and Gysel, M.: Sensitivity of the Single Particle Soot Photometer to different black carbon types, Atmos. Meas. Tech., 5, 1031–1043, doi:10.5194/amt-5-1031-2012, 2012a. 15632, 15637

Laborde, M., Schnaiter, M., Linke, C., Saathoff, H., Naumann, K.-H., Möhler, O., Berlenz, S., Wagner, U., Taylor, J. W., Liu, D., Flynn, M., Allan, J. D., Coe, H., Heimerl, K., Dahlkötter, F., Weinzierl, B., Wollny, A. G., Zanatta, M., Cozic, J., Laj, P., Hitzenberger, R., Schwarz, J. P., and Gysel, M.: Single Particle Soot Photometer intercomparison at the AIDA chamber, Atmos. Meas. Tech., 5, 3077–3097, doi:10.5194/amt-5-3077-2012, 2012b. 15629, 15637

Lack, D., Moosmüller, H., McMeeking, G., Chakrabarty, R., and Baumgardner, D.: Characterizing elemental, equivalent black, and refractory black carbon aerosol particles: a review of techniques, their limitations and uncertainties, Anal. Bioanal. Chem., 406, 99–122, doi:10.1007/s00216-013-7402-3, 2014. 15624, 15636

Lang-Yona, N., Abo-Riziq, A., Erlick, C., Segre, E., Trainic, M., and Rudich, Y.: Interaction of internally mixed aerosols with light, Phys. Chem. Chem. Phys., 12, 21–31, doi:10.1039/B913176K, 2010. 15637

Liu, D., Flynn, M., Gysel, M., Targino, A., Crawford, I., Bower, K., Choularton, T., Jurányi, Z., Steinbacher, M., Hüglin, C., Curtius, J., Kampus, M., Petzold, A., Weingartner, E., Baltensperger, U., and Coe, H.: Single particle characterization of black carbon aerosols at a tropospheric alpine site in Switzerland, Atmos. Chem. Phys., 10, 7389–7407, doi:10.5194/acp-10-7389-2010, 2010. 15635, 15636

Liu, D., Allan, J., Whitehead, J., Young, D., Flynn, M., Coe, H., McFiggans, G., Fleming, Z. L., and Bandy, B.: Ambient black carbon particle hygroscopic properties controlled by mixing state and composition, Atmos. Chem. Phys., 13, 2015–2029, doi:10.5194/acp-13-2015-2013, 2013. 15624

Matsui, H., Kondo, Y., Moteki, N., Takegawa, N., Sahu, L. K., Zhao, Y., Fuelberg, H. E., Sessions, W. R., Diskin, G., Blake, D. R., Wisthaler, A., and Koike, M.: Seasonal variation of the transport of black carbon aerosol from the Asian continent to the Arctic during the ARCTAS aircraft campaign, J. Geophys. Res., 116, D05202, doi:10.1029/2010JD015067, 2011. 15635

McMeeking, G. R., Hamburger, T., Liu, D., Flynn, M., Morgan, W. T., Northway, M., Highwood, E. J., Krejci, R., Allan, J. D., Minikin, A., and Coe, H.: Black carbon measurements in the

boundary layer over western and northern Europe, Atmos. Chem. Phys., 10, 9393–9414, doi:10.5194/acp-10-9393-2010, 2010. 15632, 15635
McMeeking, G. R., Bart, M., Chazette, P., Haywood, J. M., Hopkins, J. R., McQuaid, J. B., Morgan, W. T., Raut, J.-C., Ryder, C. L., Savage, N., Turnbull, K., and Coe, H.: Airborne measurements of trace gases and aerosols over the London metropolitan region, Atmos. Chem. Phys., 12, 5163–5187, doi:10.5194/acp-12-5163-2012, 2012. 15635
Metcalf, A. R., Craven, J. S., Ensberg, J. J., Brioude, J., Angevine, W., Sorooshian, A., Duong, H. T., Jonsson, H. H., Flagan, R. C., and Seinfeld, J. H.: Black carbon aerosol over the Los Angeles Basin during CalNex, J. Geophys. Res., 117, D00V13, doi:10.1029/2011JD017255, 2012. 15628, 15633
Moteki, N. and Kondo, Y.: Dependence of Laser-Induced Incandescence on Physical Properties of Black Carbon Aerosols: Measurements and Theoretical Interpretation, Aerosol Sci. Tech., 44, 663–675, doi:10.1080/02786826.2010.484450, 2010. 15632, 15637
Moteki, N., Kondo, Y., Miyazaki, Y., Takegawa, N., Komazaki, Y., Kurata, G., Shirai, T., Blake, D. R., Miyakawa, T., and Koike, M.: Evolution of mixing state of black carbon particles: Aircraft measurements over the western Pacific in March 2004, Geophys. Res. Lett., 34, L11803, doi:10.1029/2006GL028943, 2007. 15624, 15627
Moteki, N., Kondo, Y., and Nakamura, S.: Method to measure refractive indices of small nonspherical particles: Application to black carbon particles, J. Aerosol Sci., 41, 513–521, 2010. 15638
Moteki, N., Kondo, Y., and Adachi, K.: Identification by single-particle soot photometer of black carbon particles attached to other particles: Laboratory experiments and ground observations in Tokyo, J. Geophys. Res., 119, 1031–1043, doi:10.1002/2013JD020655, 2014. 15633
Petzold, A., Ogren, J. A., Fiebig, M., Laj, P., Li, S.-M., Baltensperger, U., Holzer-Popp, T., Kinne, S., Pappalardo, G., Sugimoto, N., Wehrli, C., Wiedensohler, A., and Zhang, X.-Y.: Recommendations for reporting "black carbon" measurements, Atmos. Chem. Phys., 13, 8365–8379, doi:10.5194/acp-13-8365-2013, 2013. 15624
Reddington, C. L., McMeeking, G., Mann, G. W., Coe, H., Frontoso, M. G., Liu, D., Flynn, M., Spracklen, D. V., and Carslaw, K. S.: The mass and number size distributions of black carbon aerosol over Europe, Atmos. Chem. Phys., 13, 4917–4939, doi:10.5194/acp-13-4917-2013, 2013. 15623, 15632, 15633
Sahu, L. K., Kondo, Y., Moteki, N., Takegawa, N., Zhao, Y., Cubison, M. J., Jimenez, J. L., Vay, S., Diskin, G. S., Wisthaler, A., Mikoviny, T., Huey, L. G., Weinheimer, A. J., and

Knapp, D. J.: Emission characteristics of black carbon in anthropogenic and biomass burning plumes over California during ARCTAS-CARB 2008, J. Geophys. Res., 117, D16302, doi:10.1029/2011JD017401, 2012. 15633, 15635
Samset, B. H., Myhre, G., Herber, A., Kondo, Y., Li, S.-M., Moteki, N., Koike, M., Oshima, N., Schwarz, J. P., Balkanski, Y., Bauer, S. E., Bellouin, N., Berntsen, T. K., Bian, H., Chin, M., Diehl, T., Easter, R. C., Ghan, S. J., Iversen, T., Kirkevåg, A., Lamarque, J.-F., Lin, G., Liu, X., Penner, J. E., Schulz, M., Seland, Ø., Skeie, R. B., Stier, P., Takemura, T., Tsigaridis, K., and Zhang, K.: Modelled black carbon radiative forcing and atmospheric lifetime in AeroCom Phase II constrained by aircraft observations, Atmos. Chem. Phys., 14, 12465–12477, doi:10.5194/acp-14-12465-2014, 2014. 15623, 15624
Schwarz, J. P., Gao, R. S., Fahey, D. W., Thomson, D. S., Watts, L. A., Wilson, J. C., Reeves, J. M., Darbeheshti, M., Baumgardner, D. G., Kok, G. L., Chung, S. H., Schulz, M., Hendricks, J., Lauer, A., Kärcher, B., Slowik, J. G., Rosenlof, K. H., Thompson, T. L., Langford, A. O., Loewenstein, M., and Aikin, K. C.: Single-particle measurements of midlatitude black carbon and light-scattering aerosols from the boundary layer to the lower stratosphere, J. Geophys. Res., 111, D16207, doi:10.1029/2006JD007076, 2006. 15624, 15627
Schwarz, J. P., Gao, R. S., Spackman, J. R., Watts, L. A., Thomson, D. S., Fahey, D. W., Ryerson, T. B., Peischl, J., Holloway, J. S., Trainer, M., Frost, G. J., Baynard, T., Lack, D. A., de Gouw, J. A., Warneke, C., and Del Negro, L. A.: Measurement of the mixing state, mass, and optical size of individual black carbon particles in urban and biomass burning emissions, Geophys. Res. Lett., 35, L13810, doi:10.1029/2008GL033968, 2008a. 15633
Schwarz, J. P., Spackman, J. R., Fahey, D. W., Gao, R. S., Lohmann, U., Stier, P., Watts, L. A., Thomson, D. S., Lack, D. A., Pfister, L., Mahoney, M. J., Baumgardner, D., Wilson, J. C., and Reeves, J. M.: Coatings and their enhancement of black carbon light absorption in the tropical atmosphere, J. Geophys. Res., 113, D03203, doi:10.1029/2007JD009042, 2008b. 15624
Schwarz, J. P., Samset, B. H., Perring, A. E., Spackman, J. R., Gao, R. S., Stier, P., Schulz, M., Moore, F. L., Ray, E. A., and Fahey, D. W.: Global-scale seasonally resolved black carbon vertical profiles over the Pacific, Geophys. Res. Lett., 40, 5542–5547, doi:10.1002/2013GL057775, 2013. 15623
Sedlacek, A. J., Lewis, E. R., Kleinman, L., Xu, J., and Zhang, Q.: Determination of and evidence for non-core-shell structure of particles containing black carbon us-

ing the Single-Particle Soot Photometer (SP2), Geophys. Res. Lett., 39, L06802, doi:10.1029/2012GL050905, 2012. 15633

Slowik, J. G., Cross, E. S., Han, J.-H., Davidovits, P., Onasch, T. B., Jayne, J. T., Williams, L. R., Canagaratna, M. R., Worsnop, D. R., Chakrabarty, R. K., Moosmüller, H., Arnott, W. P., Schwarz, J. P., Gao, R.-S., Fahey, D. W., Kok, G. L., and Petzold, A.: An Inter-Comparison of Instruments Measuring Black Carbon Content of Soot Particles, Aerosol Sci. Tech., 41, 295–314, doi:10.1080/02786820701197078, 2007. 15636

Stephens, M., Turner, N., and Sandberg, J.: Particle identification by laser-induced incandescence in a solid-state laser cavity, Appl. Optics, 42, 3726–3736, doi:10.1364/AO.42.003726, 2003. 15624, 15627

IPCC: Climate Change 2013: The Physical Science Basis. Contribution of Working Group I to the Fifth Assessment Report of the Intergovernmental Panel on Climate Change, edited by: Stocker, T. F., Qin, D., Plattner, G.-K., Tignor, M., Allen, S. K., Boschung, J., Nauels, A., Xia, Y., Bex, V., and Midgley, P., Cambridge University Press, Cambridge, United Kingdom and New York, NY, USA, 1535 pp., 2013. 15623

Stohl, A., Klimont, Z., Eckhardt, S., Kupiainen, K., Shevchenko, V. P., Kopeikin, V. M., and Novigatsky, A. N.: Black carbon in the Arctic: the underestimated role of gas flaring and residential combustion emissions, Atmos. Chem. Phys., 13, 8833–8855, doi:10.5194/acp-13-8833-2013, 2013. 15623, 15624

Svensson, J., Virkkula, A., Meinander, O., Kivekäs, N., Hannula, H.-R., Järvinen, O., Peltoniemi, J. I., Gritsevich, M., Heikkilä, A., Kontu, A., Hyvärinen, A.-P., Neitola, K., Brus, D., Dagsson-Waldhauserova, P., Anttila, K., Hakala, T., Kaartinen, H., Vehkamäki, M., de Leeuw, G., and Lihavainen, H.: Soot on snow experiments: light-absorbing impurities effect on the natural snowpack, The Cryosphere Discuss., 9, 1227–1267, doi:10.5194/tcd-9-1227-2015, 2015. 15623

Wang, Q., Jacob, D. J., Spackman, J. R., Perring, A. E., Schwarz, J. P., Moteki, N., Marais, E. A., Ge, C., Wang, J., and Barrett, S. R. H.: Global budget and radiative forcing of black carbon aerosol: Constraints from pole-to-pole (HIPPO) observations across the Pacific, J. Geophys. Res., 119, 195–206, doi:10.1002/2013JD020824, 2014a. 15623

Wang, X., Heald, C. L., Ridley, D. A., Schwarz, J. P., Spackman, J. R., Perring, A. E., Coe, H., Liu, D., and Clarke, A. D.: Exploiting simultaneous observational constraints on mass and absorption to estimate the global direct radiative forcing of black carbon and brown carbon, Atmos. Chem. Phys., 14, 10989–11010, doi:10.5194/acp-14-10989-2014, 2014b. 15623

Weingartner, E., Saathoff, H., Schnaiter, M., Streit, N., Bitnar, B., and Baltensperger, U.: Absorption of light by soot particles: determination of the absorption coefficient by means of aethalometers, J. Aerosol Sci., 34, 1445–1463, 2003. 15626

Zhang, R., Khalizov, A. F., Pagels, J., Zhang, D., Xue, H., and McMurry, P. H.: Variability in morphology, hygroscopicity, and optical properties of soot aerosols during atmospheric processing, P. Natl. Acad. Sci. USA, 105, 10291–10296, doi:10.1073/pnas.0804860105, 2008. 15624

Table 1. Extinction (b_{ext}) and absorption (b_{abs}) coefficients and backscatter fraction (b) for the five mixing state representations. Radiative forcing efficiency (RFE) is calculated using Eq. (1).

	b_{ext} (Mm^{-1})	b_{abs} (Mm^{-1})	b	RFE ($W m^{-2}$)
INT-HOM	3.98	1.58	0.09	11.20
INT-COAT	3.63	1.53	0.16	9.11
EXT-BARE	3.43	0.56	0.11	−10.93
EXT-HOM	3.58	0.79	0.11	−5.46
EXT-COAT	3.51	0.75	0.11	−6.54

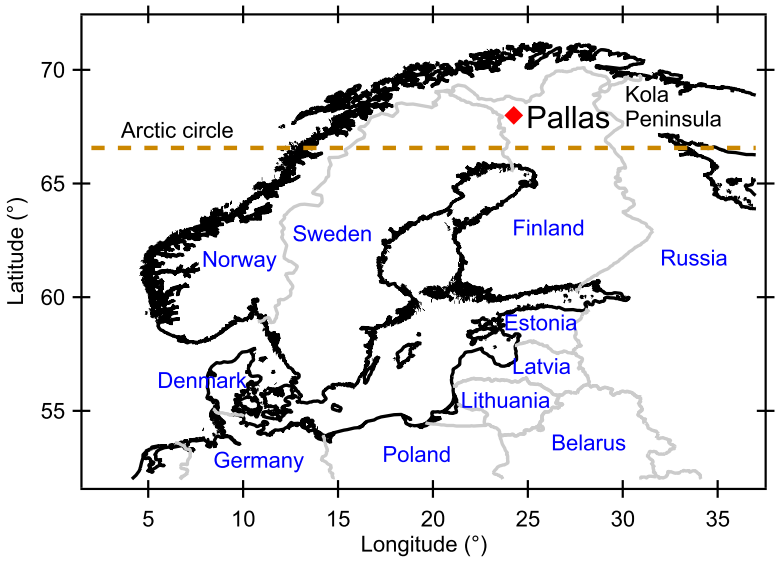

Figure 1. Location of the Pallas GAW station.

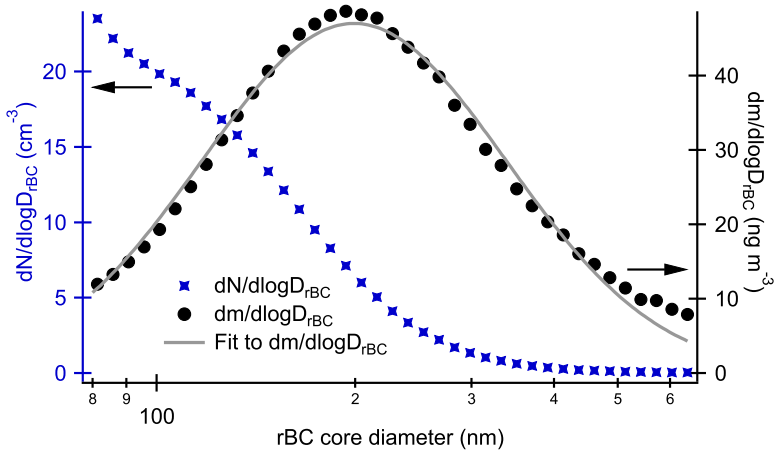

Figure 2. Campaign average rBC mass (black color, right axis) and number (blue color, left axis) size distributions. The solid gray line is a log-normal distribution fitted to the observations (geometric standard deviation is 1.70, geometric mean diameter is 199 nm and total area is 27 ng m^{-3}).

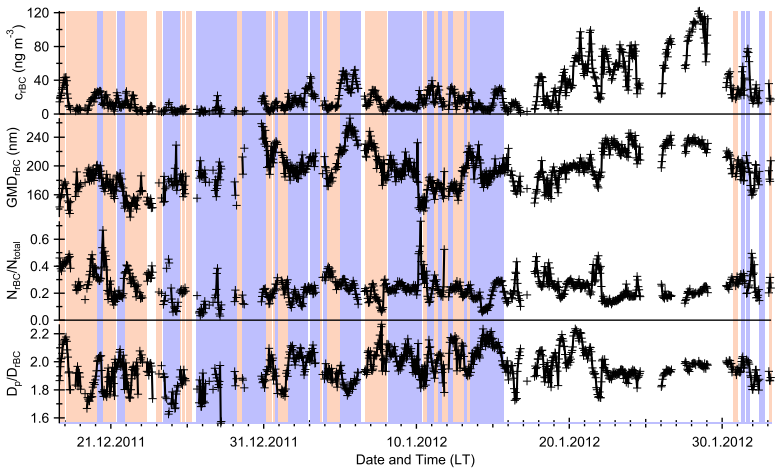

Figure 3. Time series of hourly averages of total rBC mass concentration (c_{rBC}), geometric mass mean diameter (GMD_{rBC}), the fraction of 350–450 nm particles containing rBC (N_{rBC}/N_{total}), and coated to core diameter ratio for 150–200 nm rBC cores (D_p/D_{rBC}). Blue background color indicates that the station was in cloud, red means no clouds and white means variable conditions or missing data.

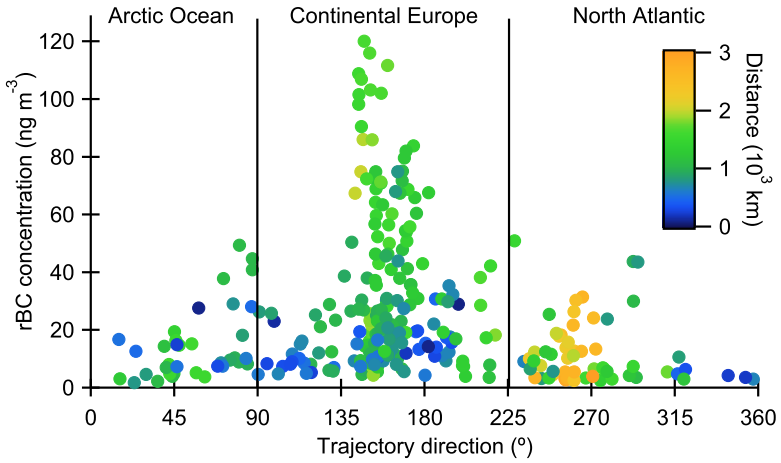

Figure 4. Total rBC mass concentration as a function of the average trajectory direction. Color scale indicates the average distance of the trajectory coordinate points from Pallas.

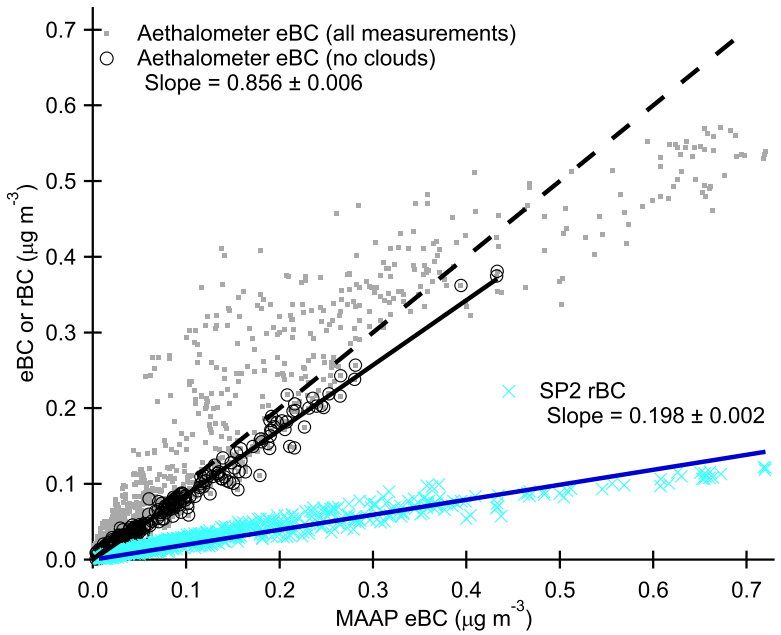

Figure 5. Aethalometer eBC (dots show all measurements and circles are those where the station is not in cloud) and SP2 rBC (crosses) as a function of MAAP eBC as well as linear fits (fixed zero offsets) to the data points. The dashed line shows 1 : 1 correlation.